AGU PUBLICATIONS

JGR

Journal of Geophysical Research: Atmospheres

RESEARCH ARTICLE
10.1002/2014JD021809

Key Points:
- Radiation is largest on south-facing canopy gaps and lowest on north-facing ones
- The effect of varying slope and aspect is greatest in large gaps
- North-facing slopes receive more energy than open canopy for a longer time

Supporting Information:
- Supporting information
- Figure S1

Correspondence to:
M. Kumar,
mukesh.kumar@duke.edu

Citation:
Seyednasrollah, B., and M. Kumar (2014), Net radiation in a snow-covered discontinuous forest gap for a range of gap sizes and topographic configurations, *J. Geophys. Res. Atmos.*, *119*, 10,323–10,342, doi:10.1002/2014JD021809.

Received 24 MAR 2014
Accepted 18 AUG 2014
Accepted article online 21 AUG 2014
Published online 15 SEP 2014

Net radiation in a snow-covered discontinuous forest gap for a range of gap sizes and topographic configurations

Bijan Seyednasrollah[1] and Mukesh Kumar[1]

[1]Nicholas School of the Environment, Duke University, Durham, North Carolina, USA

Abstract Estimating net radiation on the forest floor is crucial for predicting snowmelt recharge and for quantifying water yield from snow-dominated forested watersheds. However, complex characteristics of radiation transfer in discontinuous forest gaps make this estimation challenging. This study quantifies net radiation within a forest gap for a range of gap sizes, slopes and aspects, and meteorological conditions. The spatial distribution of net radiation in the gap is found to be heterogeneous with southern and northern areas of the gap receiving minimum and maximum energy amounts, respectively. At a midlatitude site and for completely clear sky conditions in the snow season, results suggest that net radiation in the forest gap is minimum for gaps of size equal to half of the surrounding tree height. In contrast, when sky cloudiness in the snow season is considered, net radiation shows a monotonically increasing trend with gap size. Slope and aspect of forest gap floor also impact the net radiation and its variation with gap size. Net radiation is largest and smallest on steep south-facing and north-facing slopes, respectively. Variation of net radiation with slope and aspect is largest for larger gaps. Results also suggest that net radiation in north-facing forest gaps is larger than in open areas for a longer duration in the snow season than in forest gaps on flat and south-facing slopes. Since net radiation directly affects melt recharge and evaporation, these findings have implications on forest and water management, wildfire hazard, and forest health.

1. Introduction

More than 45% of western US water supply originates in snow-fed forested uplands [*Brown et al*., 2008; *DeWalle and Rango*, 2008]. As such, accurately quantifying the magnitude and timing of melt recharge from these forested watersheds is crucial for sustainable management of water supply resources. This is however challenging due to the heterogeneity in the distribution of forest patches and gaps, which mediates snow accumulation, interception, snow-atmosphere energy exchange, and ablation rates very differently than both open areas and homogenously dense forested stands. For example, observations in a lodgepole pine (*Pinus contorta*) forest (~41°N) showed that although snow accumulation in small forest openings is larger than uniform forests, the melt rate in forest gaps is about two times greater than uniform forests [*Gary*, 1974]. Subsequent studies demonstrated that the snowmelt rate in gaps, relative to dense forest, is variable and a function of gap dimensions, with melt rates being the smallest for relatively small gaps ($D/H \approx 0.75$ to 1) and large for larger gaps ($D/H \approx 5$ to 6) [*Golding and Swanson*, 1978], where H is the height of surrounding trees and D is the gap diameter. A study in a midlatitude lodgepole pine forest (~52°N) reported the smallest ablation rates, relative to both dense forests and open areas, for forest gaps with dimensions similar to surrounding tree heights [*Berry and Rothwell*, 1992]. Measurements of snow ablation during midspring in conifer forests in Alberta, Canada, (~50°N) also showed very low snowmelt rates for small forest gaps ($D/H \approx 1$) and higher rates for very large gaps ($D/H \approx 40$) [*Bernier and Swanson*, 1993]. This paper strictly focuses on evaluating the net radiation regime in snow-covered forest gaps, which is one of the primary controls on snow disappearance timing in forest gaps.

While extensive research has been done on quantifying radiation regimes underneath a quasi-homogeneous forest with uniformly distributed trees in snow-dominated settings [e.g., *Ellis et al*., 2013; *Essery et al*., 2008b; *Hardy et al*., 2004; *Link and Marks*, 1999; *Seyednasrollah et al*., 2013; *Seyednasrollah and Kumar*, 2013; *Varhola et al*., 2010], studies regarding the estimation of radiation components in snow-covered, discontinuous forest gaps are scarce [e.g., *Pomeroy et al*., 2008; *Lawler and Link*, 2011]. A majority of work pertaining to the evaluation of radiation in discontinuous forest gaps has been limited to estimating

©2014. American Geophysical Union. All Rights Reserved.

incoming shortwave radiation and photosynthetic active radiation underneath the canopy [*de Chantal et al.*, 2003; *Huemmrich*, 2001; *Nilson*, 1971; *Song and Band*, 2004]. However, snowmelt in forest gaps is not only influenced by incoming direct shortwave radiation component but also by the diffuse and reflected (from snow) shortwave radiation (0.28–3.5 μm) and longwave radiation (3.5–100 μm) from the surrounding atmosphere and canopy, and the emitted radiation from snow surface. The shortwave and longwave radiation components also may vary from one forest gap to the next, depending on the gap size [*Lawler and Link*, 2011], height, and transmissivity of the surrounding trees [*Liang and Strahler*, 1994] which in turn may be influenced by snow interception [*Hedstrom and Pomeroy*, 1998], site topographic characteristics (slope and aspect) [*Ellis and Pomeroy*, 2007], and environmental parameters [*Berry and Rothwell*, 1992; *Susong et al.*, 1999].

This paper quantifies spatiotemporal distribution of net radiation reaching the snow-covered forest gap floor (NRSG) through development and implementation of a gap radiation model (GaRM). In many ways, this work builds on the study by *Lawler and Link* [2011], wherein all incoming radiation components were estimated along a diametrical linear transect of a level forest gap floor, under clear sky conditions. Here we use GaRM to estimate net radiation at fine temporal and spatial resolutions on the entire forest gap floor, for a range of slopes, aspects, and gap sizes, while considering site specific characteristics such as sky cloudiness, air temperature, humidity, and atmospheric transmittance. The model is then used to answer the following three questions: (i) How does gap size influence net radiation reaching the forest gap floor? (ii) What is the role of slope and aspect on the variability of net radiation with gap size? and (iii) Are forest gaps always "darker" than open areas?

2. GaRM: A Forest Gap Radiation Model

GaRM simulates spatially distributed radiation in circular clearings that are surrounded by a homogeneous dense forest. The model accounts for modification of radiation on the forest gap floor due to topographic characteristics such as slope and aspect, and for forest characteristics including canopy height and density and gap size. Net radiation (R_{Net} in W m^{-2}) on the forest gap floor is modeled as the sum of net shortwave (S_{Net} in W m^{-2}) and net longwave (L_{Net} in W m^{-2}) radiation components [*Hardy et al.*, 1997; *Pomeroy et al.*, 2009; *Sicart et al.*, 2006]:

$$R_{Net} = S_{Net} + L_{Net} \tag{1}$$

Net shortwave radiation flux on the snow surface consists of three components: incoming direct beam, $\downarrow S_{\mathrm{dir}}$ (W m^{-2}), diffuse component, $\downarrow S_{\mathrm{dif}}$ (W m^{-2}), and outgoing shortwave radiation ($\uparrow S_{\mathrm{snow}}$) from snow (W m^{-2}). The three shortwave components are evaluated using equations (2)–(4):

$$\downarrow S_{\mathrm{dir}} = S_{\mathrm{dir,\ open}} \cos\theta\, e^{-\mu L} \tag{2}$$

$$\downarrow S_{\mathrm{dif}} = \mathrm{SVF}\ S_{\mathrm{toa}}\ \tau_d\ \cos\psi\ \cos^2(\beta/2) \tag{3}$$

$$\uparrow S_{\mathrm{snow}} = \alpha \downarrow S_{\mathrm{dif}} + \alpha \downarrow S_{\mathrm{dir}} \tag{4}$$

where S_{toa} is the top-of-atmosphere solar radiation and $S_{\mathrm{dir,open}}$ is the direct shortwave radiation for open sky (W m^{-2}) which depends on time and site latitude [*Kalogirou*, 2009; *Kumar et al.*, 1997], θ is the solar incidence angle (the angle between the Sun and normal to the surface), ψ is solar zenith angle, μ is bulk canopy extinction coefficient (m^{-1}), L is the length of the solar beam passing through the canopy (m), β is the slope, τ_d is the atmospheric diffusion factor, SVF is the sky view factor, and α is the snow albedo (dimensionless). Open sky direct solar radiation, $S_{\mathrm{dir,\ open}}$ in equation (2), is calculated using the following [*Kreith and Kreider*, 2011]:

$$S_{\mathrm{dir,open}} = S_{\mathrm{toa}}\ \tau_b \tag{5}$$

where τ_b is the atmospheric transmittance for beam radiation. For clear sky conditions, atmospheric transmittance is calculated based on altitude and solar zenith angle using *Hottel* [1976]. Top-of-atmosphere solar radiation, S_{toa} in equation (5) and its variation with location and time is evaluated based on *Kalogirou* [2009]. Using direct and diffuse shortwave radiation data of clear sky days at the National Renewable Energy Laboratory site [*NREL*, 2014] in Moscow, ID, a linear regression equation (6) is derived to obtain τ_d from τ_b following the methodology presented in *Wong and Chow* [2001]:

$$\tau_d = 0.328 - 0.326\,\tau_b \tag{6}$$

©2014. American Geophysical Union. All Rights Reserved.

For cloudy sky conditions, τ_d and τ_b are directly extracted from NREL data by comparing diffuse and direct beam radiation with top-of-atmosphere radiation. Taking into account the infinitely many reflections of shortwave radiation between the snow surface on the floor and canopy [*Bohren and Thorud*, 1973], net shortwave radiation (S_{Net}) is calculated as

$$S_{\text{Net}} = \frac{\downarrow S_{\text{dir}}(1-\alpha)}{1-\alpha\alpha_c(1-\text{SVF})} + \frac{\downarrow S_{\text{dif}}(1-\alpha)}{1-\alpha\alpha_c(1-\text{SVF})} \tag{7}$$

where α_c is the canopy albedo. Estimating net longwave radiation on the snow covered forest gap floor, on the other hand, consists of adding together incoming longwave radiation from canopy, $\downarrow L_{\text{can}}$, and sky, $\downarrow L_{\text{sky}}$, and outgoing longwave radiation from snow, $\uparrow L_{\text{snow}}$. The three longwave components are evaluated using equations (8)–(10) [*Essery et al*., 2008a; *Gryning et al*., 2001; *Male and Granger*, 1981; *Marks and Dozier*, 1979; *Pluss and Ohmura*, 1997; *Pomeroy et al*., 2009; *Sicart et al*., 2006; *Todhunter et al*., 1992]:

$$\downarrow L_{\text{sky}} = \text{SVF}\ \sigma\varepsilon_{\text{sky}} {T_{\text{air}}}^4 \tag{8}$$

$$\downarrow L_{\text{can}} = (1-\text{SVF})\sigma\varepsilon_{\text{can}} {T_{\text{can}}}^4 \tag{9}$$

$$\uparrow L_{snow} = \sigma\varepsilon_{snow} {T_{snow}}^4 \tag{10}$$

where σ is Stefan-Boltzmann constant ($\sigma = 5.67 \times 10^{-8}$ W m^{-2} K^{-4}), ε_{sky} is sky emissivity, T_{air} is air temperature (K), ε_{can} is the canopy emissivity for both crown and trunk, $\varepsilon_{\text{snow}}$ is snow emissivity (dimensionless), and T_{snow} and T_{can} are snow and canopy temperatures (K), respectively. Sky and snow temperatures are assumed to be uniformly distributed across the forest gap floor. Snow surface emissivity is considered to be equal to 1.0 [*Male and Granger*, 1981], as such no reflection of the longwave components from the snow surface is considered. In the analysis, snow temperature is set to dew point temperature (T_{dp}) when $T_{\text{dp}} < 0$°C and to zero otherwise [*Andreas*, 1986].

All aforementioned formulae of individual radiation components are substituted in equation (1), to evaluate R_{Net} on the forest gap floor at any instant in time. The spatiotemporal seasonal average net radiation, defined as net snowcover radiation on the gap floor $\langle\text{NRSG}\rangle$ (W m^{-2}), is henceforth calculated using

$$\langle\text{NRSG}\rangle = \frac{\int_{t1}^{t2}\int_0^{2\pi}\int_0^{D/2} R_{\text{Net}}\ \text{d}r\ \text{d}\omega\ \text{d}t}{(t2-t1)\pi D^2/4} \tag{11}$$

where D is gap diameter and (ω, r) is the polar coordinate of a grid within the gap. The radiation calculation is performed between $t1$ and $t2$ in each control volume. Unless specified otherwise, the simulation period considered here ranges from the winter to summer solstices as it conservatively subsumes the entire duration of the snow season for many coniferous forests in mountain environments. It is assumed that snow exists on the forest gap floor for the entire snow season.

It is to be noted that in equations (1)–(11), the variables that change markedly with gap size include sky view factor (SVF), path length (L), and canopy temperature (T_{can}). Sky view factor affects longwave radiation from canopy and sky and diffuse shortwave radiation from sky. Path length, on the other hand, influences both the spatial and temporal distribution of the direct shortwave radiation. Longwave radiation from canopy is affected by canopy temperature. This indicates that $\downarrow L_{\text{sky}}$, $\downarrow L_{\text{can}}$, $\downarrow S_{\text{dir}}$, $\downarrow S_{\text{dif}}$, and $\uparrow S_{\text{snow}}$ are expected to change with gap size. The following subsections detail evaluation of the three sensitive variables and application and evaluation of the model against observed data.

2.1. Path Length of a Solar Beam Reaching the Forest Gap Floor

Path length, L, is calculated using a ray-tracing method, which involves subtraction of the length along a solar beam's path that is in the open space from the total length from the top of the canopy. For an arbitrary point, P, on the forest gap floor, with T and F being the locations where the solar beam intersects the top of the canopy and enters the clearing respectively (Figure 1), L is evaluated as

$$L = \overline{TP} - \overline{FP} = \frac{H\cos\delta(\beta,\varphi')}{\cos(\delta(\beta,\varphi')+\theta)} - \frac{\overline{BP}\cos\delta(\beta,\varphi')}{\sin\theta} \tag{12}$$

where $\overline{TP}$ is the distance along the solar beam from the top of the canopy to the forest gap floor, $\overline{FP}$ is the distance in open space, H is tree height, $\overline{BP}$ is the distance between point P and the base of the

©2014. American Geophysical Union. All Rights Reserved.

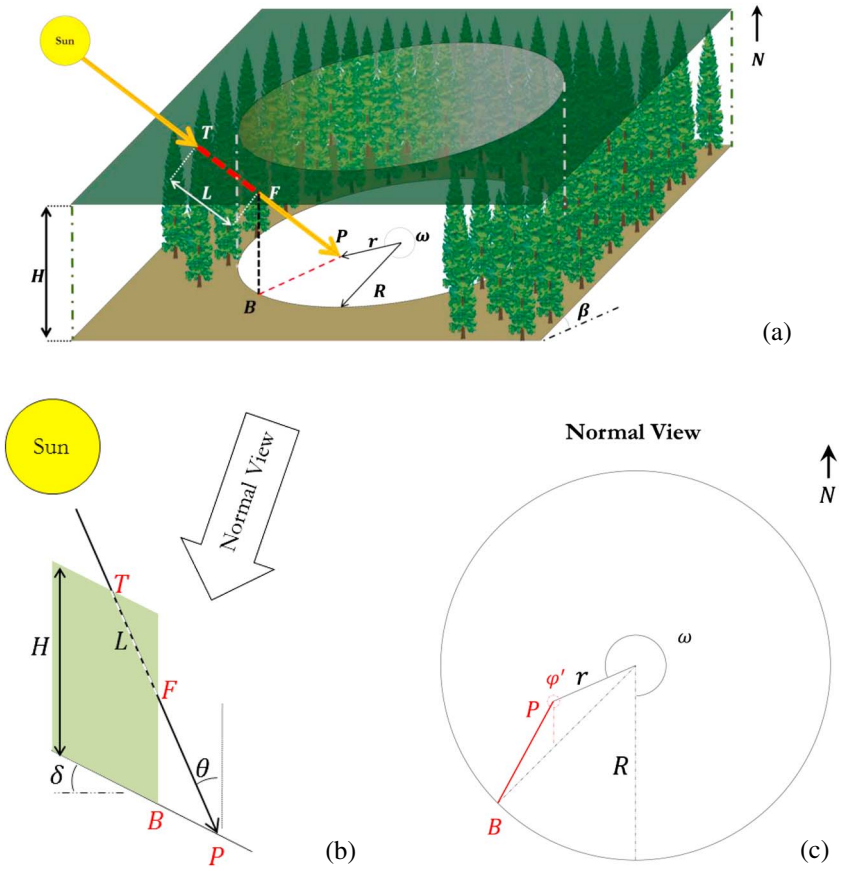

Figure 1. Schematic view of a circular forest gap located on a hillslope with slope of β and aspect of φ_s. L is the path length of a solar beam reaching the forest floor at point (r, w). $R = D/2$ is the gap radius, H is the tree height.

canopy vertically beneath point F (point B), φ' is the orientation of $\overline{BP}$ with respect to the south ($\varphi' = \tan^{-1}[\cos\beta \tan(\phi - \phi_s)]$), ϕ is solar azimuth angle, ϕ_s is the hillslope orientation with respect to the south (aspect), and $\delta(\beta, \varphi')$ is the directional slope angle (Figure 1). $\overline{BP}$ and $\delta(\beta, \varphi')$ are obtained using

$$\overline{BP} = \sqrt{R^2 - r^2 \sin^2(\omega - \varphi')} - r\cos(\omega - \varphi') \tag{13}$$

$$\delta(\beta, \varphi') = \begin{cases} -\sec^{-1}\left(\sqrt{1 + \cos^2\varphi' \tan^2\beta}\right) & \text{for } \pi/2 \le \varphi' \le 3\pi/2 \\ \sec^{-1}\left(\sqrt{1 + \cos^2\varphi' \tan^2\beta}\right) & \text{otherwise} \end{cases} \tag{14}$$

By substituting equation (13) in equation (12), path length (L) is obtained by

$$L = \frac{H\cos\delta(\beta, \varphi')}{\cos(\delta(\beta, \varphi') + \theta)} - \frac{\left[\sqrt{R^2 - r^2\sin^2(\omega - \varphi')} - r\cos(\omega - \varphi')\right]\cos\delta(\beta, \varphi')}{\sin\theta} \tag{15}$$

Shading fraction (SF) is defined as

$$\mathrm{SF} = \frac{\int_A \lfloor 1 - e^{-\mu L} \rfloor \, dA}{A} \tag{16}$$

where A is the forest gap floor area and $\lfloor\ \rfloor$ denotes the integer part function.

©2014. American Geophysical Union. All Rights Reserved.

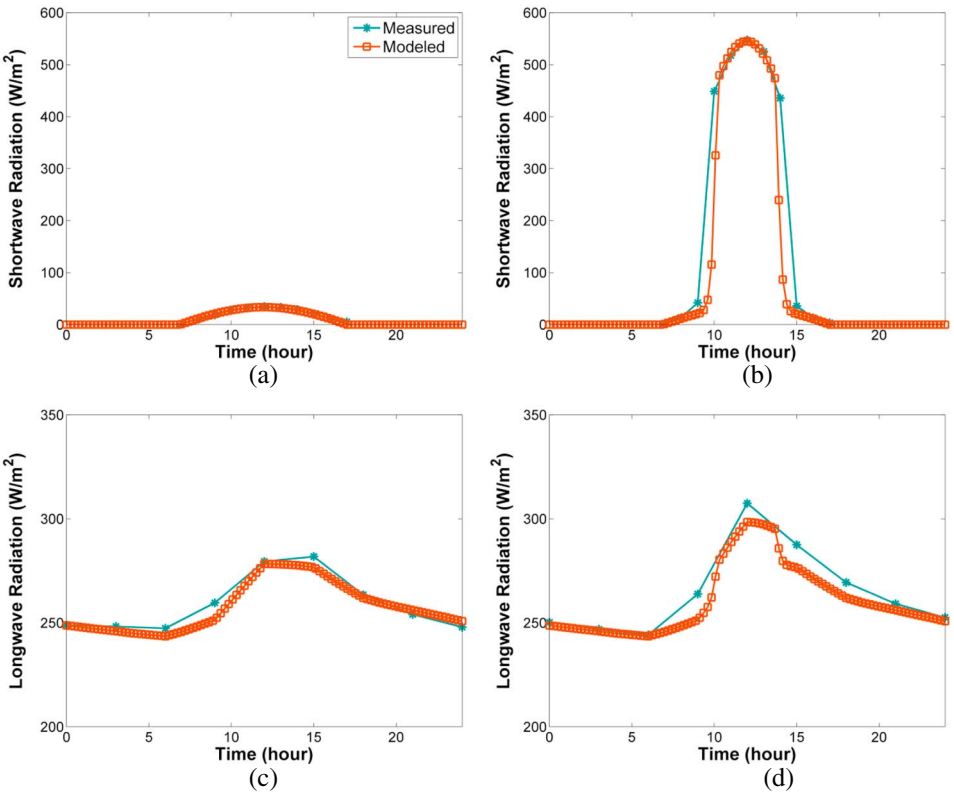

Figure 2. Comparison of modeled results against observed data at University of Idaho Experimental Watershed, near Moscow, ID on 18 February 2008: shortwave radiation at (a) southern ($R^2 = 0.98$; $\Delta = 2\%$) and (b) northern ($R^2 = 0.85$; $\Delta = 18\%$) edges of the gap and longwave radiation at (c) southern ($R^2 = 0.93$; $\Delta = 1\%$) and (d) northern ($R^2 = 0.97$; $\Delta = 2\%$) edges of the gap.

2.2. Sky View Factor

Sky view factor (SVF) is the fraction of hemispherical sky that is viewable from a given point [*Matzarakis and Matuschek*, 2011]. A three-dimensional approach is used to estimate SVF for every grid cell (r, ω) on the forest gap floor using

$$\mathrm{SVF}(r,\omega) = \frac{1}{\pi^2}\int_0^{2\pi} \tan^{-1}\left(\frac{l\cos\delta(\beta,\alpha)}{H + l\sin\delta(\beta,\alpha)}\right)\mathrm{d}\alpha \tag{17}$$

where l is the distance from the viewing point to the tree base in the direction of α which is obtained by

$$l = \sqrt{R^2 - r^2\sin^2(\omega-\alpha)} - r\cos(\omega-\alpha) \tag{18}$$

The spatially averaged sky view factor of forest gap (GSVF), is defined as

$$\mathrm{GSVF} = \frac{1}{\pi R^2}\int_0^{2\pi}\int_0^{R}\mathrm{SVF}(r,\omega)r\,\mathrm{d}r\,\mathrm{d}\omega \tag{19}$$

2.3. Canopy Temperature

During high-insolation conditions, canopy temperature can exceed air temperature by about 1–2 K [*Pomeroy et al.*, 2009]. As solar radiation is the dominant control on the temperature difference between tree and air, temperature is expected to be higher for trees that are exposed to the solar radiation in relation to shaded trees. Here we develop a regression between radiation at the gap edge and difference between T_{air} and T_{can}. Using observed longwave radiation data at the northernmost edge of the gap for calibration (see Figure 2d), ($T_{can} - T_{air}$) is set equal to 2 K per shortwave radiation of 150 W m^{-2} at the gap edge. The variation of T_{can} with azimuth is accounted for while estimating $\downarrow L_{can}$ at any grid cell within the gap.

©2014. American Geophysical Union. All Rights Reserved.

Table 1. Parameters Used in the Gap Radiation Model

Quantity	Value
Minimum snow albedo (α_{min})	0.35
Maximum snow albedo for fresh snow (α_{max})	0.85
Snow free canopy albedo (α_c)	0.2
Snow emissivity (ε_{snow})	1.0
Canopy emissivity (ε_{can})	0.98
Canopy extinction coefficient (μ)	0.3 m^{-1}

2.4. Model Application and Evaluation at the Control Site

Representative values of physical parameters including ε_{snow}, ε_{can}, and α_c are used to calculate the radiation components. Typical values of snow albedo and emissivity of canopy, sky and snow are listed in Table 1. The snow albedo time series is calculated using a decay model [*Sproles et al*., 2013; *Strack et al*., 2004]:

$$\alpha_t = \alpha_{t-1} - \tau_{nm}\delta t \tag{20}$$

for nonmelting conditions and

$$\alpha_t = (\alpha_{t-1} - \alpha_{min})\exp(\tau_m \delta t) + \alpha_{min} \tag{21}$$

for melting conditions. α_t and α_{t-1} are snow albedo (dimensionless) for the next and current time steps, respectively, α_{min} is the minimum snow albedo (dimensionless), δt is time step size with respect to a day (dimensionless) and τ_{nm} = 0.008 and τ_m = 0.024 are the decay rates for nonmelting and melting conditions. Melting conditions are defined based on whether daily air temperature is above 0°C [*Douville et al*., 1995]. The maximum snow albedo is set to 0.85 for fresh snowfall (25 mm). An intermediate value of α_{min} = 0.35 (*Sproles et al*. [2013] suggested α_{min} of 0.5 for open areas and 0.2 for forested regions) is used for the minimum snow albedo in the discontinuous forest gap. Snow albedo obtained based on equations (20) and (21) is adjusted to account for variations in solar incidence angle (θ) using *Gardner and Sharp* [2010]:

$$\alpha_{mod} = \alpha + 0.53\,\alpha(1-\alpha)(1-\cos\theta)^{1.2} \tag{22}$$

where α_{mod} is the modified snow albedo for direct shortwave radiation. The representative albedo time series (see Figure S1 in the supporting information) that is eventually used in equation (7) to evaluate S_{Net} is obtained by averaging 54 years (1960–2014) of albedo series modeled using equations (20)–(22). Canopy albedo is set to 0.2 [*Bohren and Thorud*, 1973; *Eck and Deering*, 1990, 1992]. The emissivity of snow and canopy are set to 1.0 [*Dozier and Warren*, 1982; *Sicart et al*., 2006; *Warren*, 1982] and 0.98 [*Pomeroy et al*., 2009], respectively. Daily clear sky emissivity ($\varepsilon_{sky,\,clear}$), which depends on air temperature, vapor pressure, and humidity [*Marthews et al*., 2012], is estimated using [*Prata*, 1996]:

$$\varepsilon_{sky,\,clear} = 1 - (1+w)e^{-\sqrt{1.2+3w}} \tag{23}$$

where w is precipitable water in the air (cm) and calculated as $w \cong 465\left(\frac{e_0}{T_{air}}\right)$, e_0 is ambient vapor pressure (kpa) and T_{air} is screen level air temperature (K). Cloudy sky emissivity ($\varepsilon_{sky,\,cloudy}$) is obtained using the Kimball correction method [*Kimball et al*., 1982], which accounts for cloud elevation and base temperature. The Kimball correction model has been noted to perform particularly well within North America [*Flerchinger et al*., 2009].

The variation of NRSG in relation to forest gap size is calculated in a coniferous forest stand near Moscow, ID (46.8°N, 116.9°W). The site is located within midlatitude coniferous forests in North America, where there is a considerable interest in understanding the role of forest heterogeneity on seasonal snow energetics. In this analysis, we use a representative tree height of 25 m for the site and an estimated canopy extinction coefficient (μ) of 0.3 m^{-1}. Relevant input data pertaining to air temperature and relative humidity are obtained from the National Climatic Data Center meteorological station near Moscow, ID [*NCDC*, 2014]. Cloud cover data are obtained from the National Renewable Energy Laboratory [*NREL*, 2014]. The site has long-term air temperature (1973–2013) and solar radiation (1990–2010) data.

All the radiation components (equation (1)) are calculated on a polar coordinate discretized gridded floor (180 × 50) within a circular gap of diameter, D. Scenario simulations are performed for D ranging from 0.1H to 20H. The average net radiation is then calculated for the entire gap from 21 December to 20 June using equation (11) at 10 min intervals.

Simulated incoming shortwave and longwave radiation components obtained from GaRM are validated at a mixed coniferous forest site in University of Idaho Experimental Forest, near Moscow, Idaho (46°51′16″N, 116°43′24″W, elevation = 884 m). The circular forest gap (D = 60 m) at the site is surrounded by dense

©2014. American Geophysical Union. All Rights Reserved.

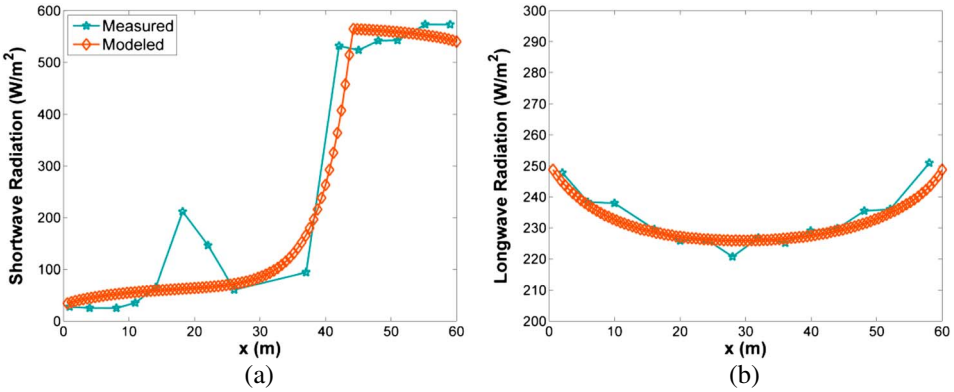

Figure 3. Validation of the Gap Radiation Model (GaRM) against the measured data at University of Idaho Experimental Watershed, near Moscow, ID on 18 February 2008 along the south-north forest gap transect: (a) shortwave radiation at the solar noon ($R^2 = 0.93$; $\Delta = 1\%$) and (b) longwave radiation at the midnight ($R^2 = 0.93$; $\Delta = 5\%$); $x = 0$ represents the southern point of the forest gap and $x = 60$ m represents the northern point of the forest gap.

stands of western red cedar (*Thuja plicata*) trees with an average tree height of 25 m. The modeled incoming shortwave ($\downarrow S_{dir} + \downarrow S_{dif}$; equations (2)–(6)) and longwave ($\downarrow L_{sky} + \downarrow L_{can}$; equations (8) and (9)) radiation components are compared against the observed data at both southern and northern edges of the forest gap. The modeled shortwave radiation reasonably matches both the temporal variation ($R^2 = 0.98$ and 0.85 for the southern and northern edges, respectively) and the mean of the observed data. The difference between the modeled and observed estimates of total shortwave radiation is equal to 2% (~0.2 W m^{-2}) and 18% (~19 W m^{-2}) of the observations at the southern and northern edges, respectively (Figures 2a and 2b). The comparisons of longwave radiations between the model and the observations also show excellent correlations ($R^2 = 0.93$ and 0.97 for the southern and northern edges, respectively). Moreover, the differences in total longwave radiation estimates from the model and observations are minuscule ($\Delta = 1\%$ or ~3 W m^{-2}, and 2% or ~6 W m^{-2}, for the southern and northern edges of the gap, respectively; Figures 2c and 2d). Spatial variations of radiation components are also compared against the observed data at solar noon for shortwave radiation and at midnight for longwave radiation on 18 February 2008. Although shortwave radiation shows a strong spatial gradient at the site, the model was able to properly capture the variation along the south-north transect ($R^2 = 0.93$). The difference in the total shortwave radiation from the model and observations are also nominal ($\Delta = 1\%$ or ~3 W m^{-2}; Figure 3a). Divergence between observed and model results is seen at a distance of around 20 m from the southern edge of the gap, where observed data show a sudden jump. This is likely due to holes and heterogeneities in the surrounding canopy, which are not resolved within a hemispherical photograph, and hence not accounted for in the model simulation. Simulated longwave radiation components also show sufficient consistency with the observed data ($R^2 = 0.93$ and difference in the total longwave radiation, $\Delta = 5\%$, or ~12 W m^{-2}; Figure 3b). Readers are referred to *Lawler and Link* [2011] for more details of the observation experiment setup.

3. Results and Discussion

The results are presented thematically, following the questions outlined previously.

3.1. How Gap Size Influences Net Radiation Reaching the Forest Gap Floor

All radiation components (equation (11)) vary spatially on the forest gap floor. Spatial variability of radiation components, in both clear and cloudy sky conditions, are further analyzed by performing GaRM simulations for an intermediate-sized forest gap ($D/H = 4$) on a level forest. The two incoming shortwave radiation components ($\downarrow S_{dir}$ and $\downarrow S_{dif}$) vary differently within the forest gap. Direct shortwave radiation is mainly affected by shadow patterns, which in turn are affected by variations of Sun position. For level forest gaps located in the Northern Hemisphere, the southern edge is shaded during most of the day. As a result, it receives very small direct shortwave radiation. With increasing distance from the southern edge of the gap, the seasonal average direct shortwave radiation gradually increases. Very near to the northern edge of the gap, however, the seasonal direct shortwave radiation reduces a bit, due to shading by neighboring trees

©2014. American Geophysical Union. All Rights Reserved.

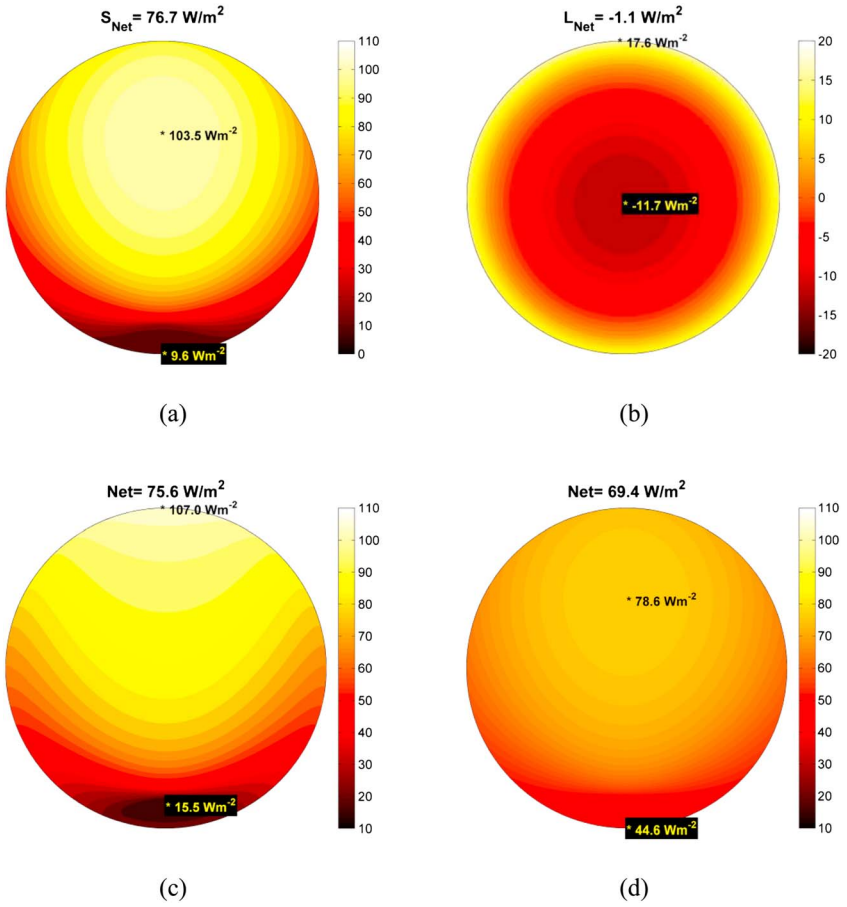

Figure 4. Spatial variation of seasonally averaged radiation on a level forest gap (D/H = 4): (a) shortwave radiation in clear sky conditions, (b) longwave radiation in clear sky conditions, (c) net radiation in clear sky conditions, and (d) net radiation in interspersed cloudy sky conditions.

located along the eastern/western edge of the gap in early/late hours of the day. Therefore, direct shortwave radiation is maximum at a distance = 0.25D from the center of the gap toward the northern edge. The diffuse part of shortwave radiation ($\downarrow S_{dif}$) varies within the forest gap due to variation in sky view factor (equation (3)), which is maximum at the center of the forest gap. $\downarrow S_{dif}$ radially decreases to its minimum value near the edge of the gap. Since the spatial gradient of $\downarrow S_{dir}$ within the gap is much more than that of $\downarrow S_{dif}$ (~11 times greater under clear sky conditions), $\downarrow S_{dir}$ dominates the variations of total incoming shortwave radiation. As the reflected shortwave radiation from snow ($\uparrow S_{snow}$) is proportional to the total incoming shortwave radiation, the spatial variation of seasonal average net shortwave radiation, S_{Net}, follows the variation pattern of $\downarrow S_{dir}$ with its magnitude ranging from 9.6 W m^{-2} near the southern edge to 103.5 W m^{-2} at a point close to 0.25D from the center of the gap toward the northern edge. With increasing distance from the point of maximum S_{Net} toward the western and eastern edges, S_{Net} decreases monotonically. Spatially averaged seasonal S_{Net} received in the forest gap of size D/H = 4 is equal to 76.7 W m^{-2} (Figure 4a).

The three longwave radiation components (equation (8)) also exhibit markedly different variations on the forest gap floor. $\downarrow L_{can}$ and $\downarrow L_{sky}$ are influenced by variations in sky view factor (equations (8) and (9)). $\downarrow L_{sky}$ is directly proportional to sky view factor and hence expresses concentric variations on the forest gap floor with a maximum value obtained at gap center. In contrast, anisotropic variability of canopy temperature along the gap circumference causes a slightly eccentric (off center) variability in $\downarrow L_{can}$. Since $\downarrow L_{can}$ varies conversely to sky view factor and T_{can} is maximum at the northernmost edge of the gap, minimum value of $\downarrow L_{can}$ is obtained slightly south of the gap center. $\uparrow L_{snow}$, on the other hand, is spatially uniform within the gap, as snow temperature is assumed to be the same everywhere. Since canopy emissivity and temperature are larger than sky emissivity and temperature, variations in $\downarrow L_{can}$ within the gap is larger than

©2014. American Geophysical Union. All Rights Reserved.

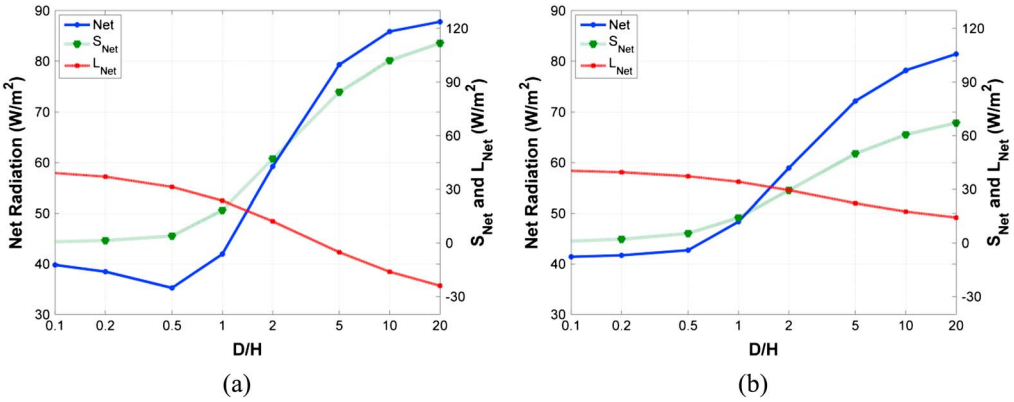

Figure 5. Variation of radiation components with gap size on a level forest floor: (a) for completely clear sky conditions during snow season and (b) when sky cloudiness at the site is considered. All radiation values are averaged over the winter to summer solstices period.

variations in $\downarrow L_{sky}$. As a result, spatial variation in net longwave radiation is controlled by $\downarrow L_{can}$. This also results in minimum net longwave radiation to be expressed slightly south of the gap center and maximum on the northern edge. Seasonal average L_{Net} received in an intermediate forest gap ($D/H = 4$) is simulated to be equal to -1.1 W m^{-2} (Figure 4b).

For the studied forest gap ($D/H = 4$), spatial variation in S_{Net} is larger than the variations in L_{Net} (e.g., $\Delta S_{Net} \approx 94$ W m^{-2} compared to $\Delta L_{Net} \approx 29$ W m^{-2}). Hence, the spatial gradient of NRSG is controlled by S_{Net}, except at locations closer to the southern edge, which are shaded at all times during the season. For the snow season with completely clear sky conditions (Figure 4c), NRSG is maximum ($\approx$107 W m^{-2}) at the northernmost location of the gap and minimum ($\approx$15 W m^{-2}) close to the southern edge of the gap. For the case in which interspersed sky cloudiness at the site during the snow season is considered, (Figure 4d), the spatial pattern of S_{Net} is similar to that in the clear sky case; however, its magnitude is much less. On the other hand, due to the high thermal emissivity of cloudy sky, longwave radiation on the forest gap floor is larger in this case. As a result, the range of NRSG within the forest gap is relatively smaller (45 W m^{-2} to 79 W m^{-2}), with its mean being 10% less than that in clear sky conditions. Notably, net shortwave radiation is still relatively larger than net longwave radiation at the site, resulting in spatial variation of NRSG to follow a spatial pattern that is exhibited by S_{Net}.

The shortwave and longwave radiation components, and hence the NRSG, on the forest gap floor vary with gap size. As gap size increases, shading fraction on the forest gap floor decreases and hence direct shortwave radiation ($\downarrow S_{dir}$) increases. The diffuse shortwave radiation ($\downarrow S_{dif}$) also increases with increasing gap size due to the increase in the viewable portion of sky (SVF). Since reflected shortwave radiation from snow is the fractional sum of $\downarrow S_{dir}$ and $\downarrow S_{dif}$ (equation (4)), $\uparrow S_{snow}$ also increases with increasing gap size. As a result, S_{Net} monotonically increases with increasing gap size (D/H). The three longwave radiation components ($\uparrow L_{snow}$, $\downarrow L_{sky}$, and $\downarrow L_{can}$) vary differently with changes in gap size. The emitted longwave radiation from snow is independent of gap size (equation (10)). Incoming longwave radiation from sky is directly proportional to sky view factor and hence increases with increasing gap size. However, incoming radiation from the canopy is conversely related to SVF, leading to a monotonically decreasing behavior with increasing gap size. Since the decrease in $\downarrow L_{can}$ is larger than the increase in $\downarrow L_{sky}$, mostly because canopy emissivity (ε_{can}) is larger than sky emissivity (ε_{sky}), net longwave radiation (L_{Net}) monotonically decreases with gap size.

In snow seasons with completely clear sky conditions (Figure 5a), the increasing trend in S_{Net} and the decreasing trend in L_{Net} with D/H lead to a nonmonotonic variation in NRSG. For gap sizes $D/H < 0.5$, as gap size increases, L_{Net} decreases more rapidly than the increase in S_{Net}, resulting in a decreasing NRSG with gap size. For gap sizes $D/H > 0.5$, NRSG shows an increasing trend with gap size. Because of similar changes in S_{Net} and L_{Net} in very large gaps ($D/H > 10$), changes in the two energy components negate each other, thus resulting in NRSG to become less sensitive to gap size. A decreasing followed by an increasing trend in NRSG leads to a minimum seasonal average net radiation at $(D/H)_{min} = 0.5$. The minimum net

©2014. American Geophysical Union. All Rights Reserved.

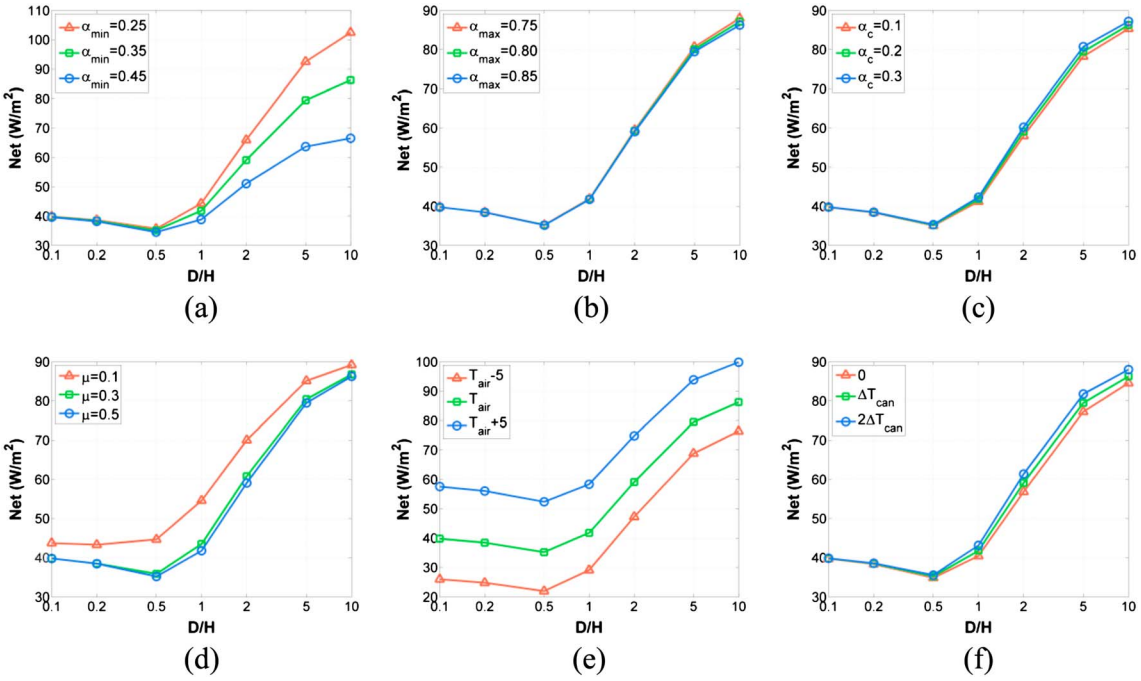

Figure 6. Sensitivity of NRSG in clear sky conditions to: (a) minimum and (b) maximum snow albedos, (c) canopy albedo, (d) canopy extinction coefficient, (e) air temperature, and (f) the difference between canopy and air temperatures. In all the figures, the middle curve represents the baseline results presented earlier in the text. All radiation values are averaged over a period spanning from the winter to summer solstice.

radiation ($NRSG_{min}$) is about 11% less than the net radiation in very small gaps ($NRSG_{sgap}$) and about 60% less than the net radiation received in very large gaps and open areas ($NRSG_{lgap}$).

For snow seasons with interspersed cloudy conditions, sky cloudiness affects both shortwave and longwave radiation components. Atmospheric scattering and absorption of solar radiation increases in the presence of clouds, resulting in a decrease in $\downarrow S_{dir}$ and an increase in $\downarrow S_{dif}$. In spite of the increase in diffuse part of shortwave radiation in cloudy sky conditions, the total incoming shortwave radiation and, hence, S_{Net} decreases. The decrease in S_{Net} is significant in large forest gaps and almost negligible in very small gaps as shading fraction is close to 100% in the latter case. Sky cloudiness influences longwave radiation by increasing sky emissivity and $\downarrow L_{sky}$ while $\downarrow L_{can}$ experiences a minor change, resulting in an increase in L_{Net}. The increase in L_{Net} is proportional to sky view factor and, therefore, the increase in longwave radiation is larger in open areas and large forest gaps rather than small gaps, where sky view factor is small. Simulation results (Figure 5b) at the study site show that in small ($D/H < 1$) and large ($D/H > 10$) gaps, the increase in S_{Net} with D/H is neutralized by the decrease in L_{Net}, leading to a muted sensitivity in NRSG to D/H. In intermediate gap sizes ($1 \leq D/H \leq 10$), the increase in S_{Net} is larger than the decrease in L_{Net}, resulting in an increasing NRSG with D/H.

It is to be noted that the results for interspersed cloudy sky condition is obtained using the site-corrected sky emissivity in cloudy conditions (suggested for North American sites by *Flerchinger et al.* [2009]) and are dependent on site specific characteristics including cloud cover and sky emissivity. Larger sky emissivity or higher cloud cover is expected to result in larger longwave radiation, particularly in larger gaps. This may cause a reduction in the rate of change of longwave radiation with gap size, thus resulting in a monotonically increasing NRSG with gap size. In contrast, lower-site sky emissivity and cloud cover may result in a nonmonotonic trend of NRSG with gap size thus leading to a radiation minimum at an intermediate gap size. The magnitude and variations in NRSG are also dependent on representative values of parameters such as α_{min}, α_{max}, α_c, and μ. Higher values of α_{min} lead to a higher seasonal albedo, which results in a reduction of S_{Net} and NRSG. The decrease is higher for larger gaps where the shortwave component is dominant (Figure 6a). Notably, an increase in α_{max} also results in similar variations in NRSG. However, variations in NRSG are almost negligible in this case (Figure 6b). This is because the albedo decreases rapidly with time after a snowfall event. The albedo decay period dominates the shortwave radiation energetics both in terms

©2014. American Geophysical Union. All Rights Reserved.

of its duration and periods of high incoming radiation intensity. Sensitivity of NRSG estimates to α_c and μ has been plotted in Figures 6c and 6d. Considering all other parameters to be the same, an increase in α_c (for example, in cases where intercepted snow remains on the canopy for a longer period of time) results in slightly larger shortwave radiation and hence larger NRSG. But the variations in NRSG are very modest. In contrast, while a larger canopy extinction coefficient (e.g., denser forest surrounding the gap) causes a small decrease in S_{Net} and NRSG, a smaller μ results in a significant increase in NRSG. To sum up, among the four model parameters considered here, NRSG is almost insensitive to α_{max} and α_c for the examined ranges. On the other hand, sensitivities to α_{min} and μ are mostly apparent for gaps of size larger than $D/H \geq 1$ and with $\mu = 0.1$, respectively. Notably, NRSG shows nonmonotonic variations with gap size for all the considered parameter ranges, with $\mu = 0.1$ being an exception in which case NRSG shows an increasing trend. Sensitivity of NRSG and its variation with gap size is also evaluated for a range of air and canopy temperatures. A warmer snow season results in an increase in both canopy and snow temperatures, leading to an increase in all longwave radiation components (see equations (8)–(10)). Higher air temperatures during the snow season lead to an almost uniform increase in NRSG for all gap sizes (Figure 6e). In contrast, for warmer canopy temperatures with temperature difference between canopy and air temperature being equal to two times the difference considered in the base simulation, the increases in L_{Net} and NRSG are greater for larger gap sizes because of higher insolation on canopy in larger gaps (see Figure 5a). Along similar lines, for colder canopy temperature conditions ($T_{can} = T_{air}$, i.e., $\Delta T_{can} = 0$), L_{Net} and hence NRSG decreases, and the decrease is greater in larger gaps (Figure 6f). To sum up, the sensitivity of seasonal net radiation (NRSG) to canopy temperature is almost negligible in smaller gaps and significant in gaps of size $D/H \geq 1$.

3.2. Effects of Slope Angle on Net Radiation in Forest Gaps

In order to understand the impact of slope on net radiation reaching the forest gap floor and its variations with gap size, NRSG is calculated for a range of D/H values on an inclined south-facing hillslope. Four different slope angles (0°, 15°, 30°, and 45°) are considered. The maximum considered slope angle is limited to 45°, since forests are uncommon on very steep hillslopes. Changes in slope angle influence both shortwave and longwave radiation components by affecting solar incidence angle (θ), shading fraction (SF), and sky view factor (SVF).

For all south-facing slope angles considered in this study, shading fraction (SF) decreases with increasing gap size because of the decrease in solar incidence angle (θ). Since both θ and SF decrease with increasing slope angle on a south-facing hillslope, $\downarrow S_{dir}$ is larger for higher slopes (see equation (2)). $\downarrow S_{dif}$, on the other hand, experiences a small decrease with slope angle due to a decreasing sky view factor (see equation (2)). Since the increase in $\downarrow S_{dir}$ is much larger than the change in $\downarrow S_{dif}$, and $\uparrow S_{snow}$ is only a fraction of the sum of $\downarrow S_{dir}$ and $\downarrow S_{dif}$, S_{Net} follows the trend of $\downarrow S_{dir}$ and increases with increasing slope angle (Figure 7a). $\downarrow L_{sky}$ and $\downarrow L_{can}$ radiation components also change with slope angle due to the influence on SVF (see equations (8) and (9)), which decreases with slope angle especially in small gaps [*Seyednasrollah et al.*, 2013]. $\uparrow L_{snow}$, on the other hand, is independent of slope angle (see equation (10)). Since $\downarrow L_{can}$, which varies proportionally to $\downarrow S_{dir}$ (because of its role in increasing canopy temperature) and conversely to SVF, determines the variation of L_{Net} with increasing slope angle, L_{Net} is larger for steeper forests (with smaller SVF and larger $\downarrow S_{dir}$) in gaps of size $D/H < 5$. In large gaps ($D/H > 5$), sky view factor and hence L_{Net} are almost insensitive to increasing slope angle (Figure 7b).

In clear sky conditions, the rate of change in S_{Net} with increasing slope angle is much larger than the rate of change in L_{Net}. Therefore, NRSG monotonically increases with increasing slope angle for all gap sizes. The increase in NRSG with slope angle is substantial for intermediate to large gaps ($D/H > 1$), while it slightly decreases for small gaps of size $D/H < 0.5$ (Figure 7c). As a result, the minimum radiation, $NRSG_{min}$ is expressed at $D/H = 0.5$ for all considered slope angles. However, the ratio of $NRSG_{min}$ to $NRSG_{sgap}$ keeps increasing from 89% to 93% with an increase in slope angle from 0° to 45° (see Table 2).

For the case when cloudiness of sky during the snow season is considered, NRSG increases with increasing slope angle from level forest gaps to 30° slope angle for all gap sizes (Figure 7d). For steeper slopes (>30°), the increase in NRSG is modest for forest gaps of size $D/H < 10$ and almost negligible for large forest gaps ($D/H > 10$). The results also show that $(D/H)_{min}$ remains almost the same with increasing slope angle in interspersed cloudy sky conditions (see Table 2). It is to be noted that theoretically, increasing slope angle pushes $(D/H)_{min}$ to smaller gap dimensions, even though it is too little to be apparent at this site.

©2014. American Geophysical Union. All Rights Reserved.

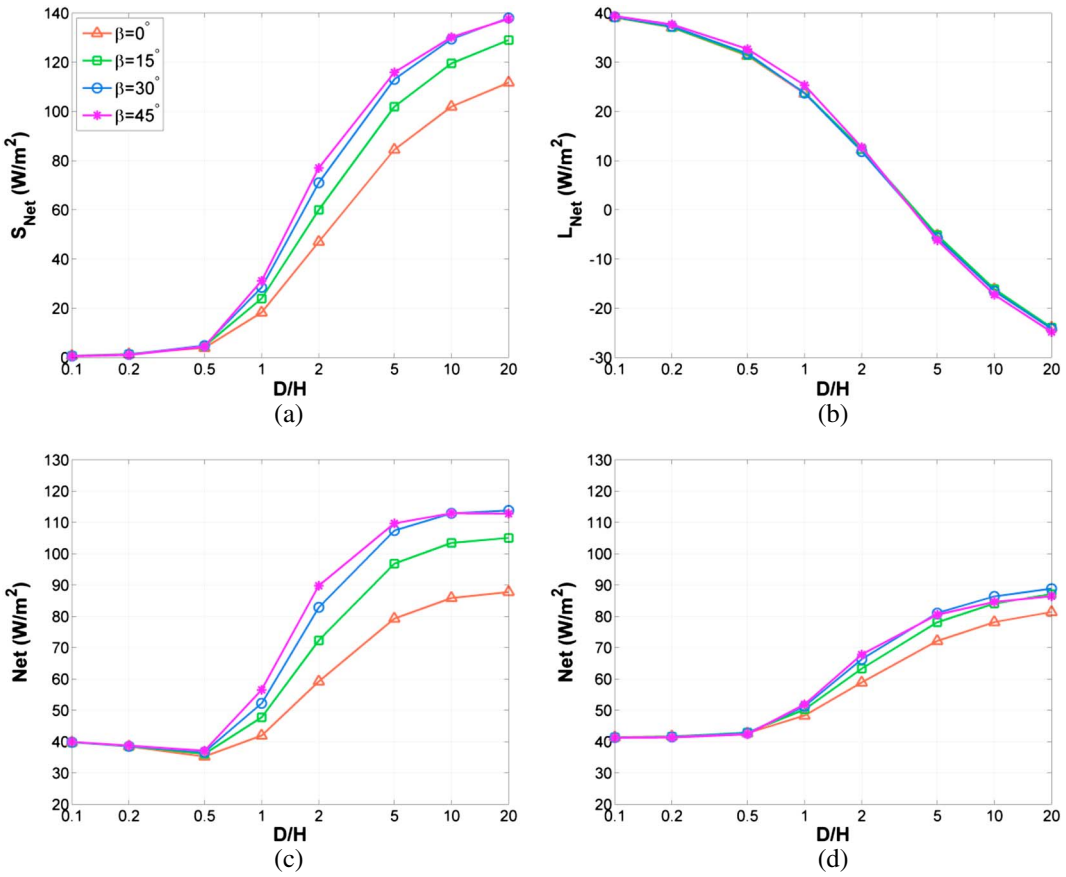

Figure 7. Effect of slope on the variation of radiation with gap size on a south-facing forest floor: (a) Net shortwave radiation in clear sky conditions, (b) net longwave radiation in clear sky conditions, (c) net radiation in clear sky conditions, and (d) net radiation when sky cloudiness is considered. All radiation values are averaged over a period spanning from the winter to summer solstices.

3.3. Effect of Hillslope Orientation on Net Radiation in Forest Gaps

The influence of aspect on the variation of NRSG with gap dimension is investigated by performing GaRM simulations on a 15° hillslope for five different aspects: south, southwest/southeast, west/east, northwest/northeast, and north. Changing the aspect of the forest gap floor influences direct shortwave radiation ($\downarrow S_{dir}$) by altering the incidence angle and path length of the solar beam. The incidence angle increases for northward facing aspects [*Seyednasrollah et al.*, 2013], which translates to reduction in the intensity of $\downarrow S_{dir}$. Furthermore, as incidence angle increases, path length and hence shading fraction increase too, resulting in a rapid decrease in $\downarrow S_{dir}$. Since changes in aspect do not cause any change in sky view factor,

Table 2. Statistics of Minimum Net Radiation for a Range of South-Facing Slopes

Sky Condition	Slope Angle	$(D/H)_{min}$	Proportion of Radiation in Relation to Very Small Gaps (%)	Proportion of Radiation in Relation to Very Large Gaps (%)
Clear sky	0°	0.5	89	40
	15°	0.5	91	34
	30°	0.5	82	32
	45°	0.5	93	32
Interspersed cloudy	0°	0.1	100	51
	15°	0.1	100	47
	30°	0.1	100	46
	45°	0.1	100	47

©2014. American Geophysical Union. All Rights Reserved.

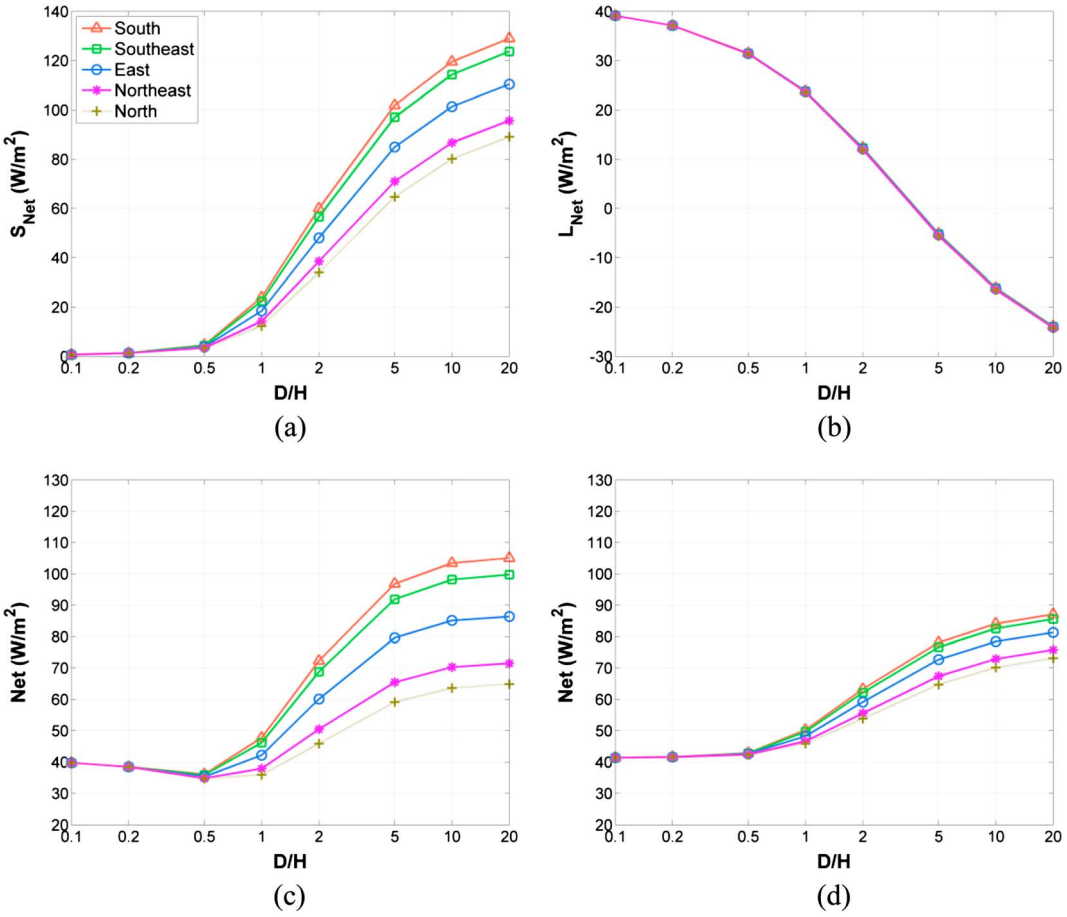

Figure 8. Effect of aspect on the variability of radiation with gap size on a sloping (angle = 15°) forest gap: (a) Net shortwave radiation in clear sky conditions, (b) net longwave radiation in clear sky conditions, (c) net radiation in clear sky conditions, and (d) net radiation when sky cloudiness is considered. All radiation values are averaged over a period spanning from the winter to summer solstices.

$\downarrow S_{dif}$ is insensitive to changes in aspect. As $\uparrow S_{snow}$ is proportional to $\downarrow S_{dir} + \downarrow S_{dif}$, it decreases with northward changing aspect. Based on the aforementioned variations in $\downarrow S_{dir}$, $\downarrow S_{dif}$, and $\uparrow S_{snow}$, net shortwave radiation decreases with aspects changing from south-facing to north-facing orientations (Figure 8a). In contrast, among the three longwave radiation components ($\downarrow L_{can}$, $\downarrow L_{sky}$, and $\uparrow L_{snow}$), $\downarrow L_{can}$ shows a minor decrease for northward facing aspects whereas $\downarrow L_{sky}$ and $\uparrow L_{snow}$ are insensitive to changing aspect. The decrease in $\downarrow L_{can}$ for northward aspects is because of reduction in shortwave radiation, which then results in a decrease in the temperature of radiation-exposed canopy. Since the change in $\downarrow L_{can}$ is very small, net longwave radiation for different aspects are almost identical (Figure 8b). As the decrease in S_{Net} is much larger than the changes in L_{Net}, net radiation monotonically decreases with increasing hillslope aspect toward north. The decrease in NRSG due to changing aspect is larger in large forest gaps (Figure 8c). The sensitivity of NRSG to changing aspect is negligible in very small gaps ($D/H < 0.5$). The results show that the minimum radiation is observed for $(D/H)_{min}$ ranging from 0.5 to 1.0, with larger $(D/H)_{min}$ on north-facing slopes. For snow seasons with completely clear sky conditions, the proportion of $NRSG_{min}$ in relation to $NRSG_{sgap}$ monotonically decreases with aspect changing from the south toward the north. For instance, the ratio decreases from about 91% in south-facing forest gaps to about 89% in east/west-facing hillslopes and then to about 87% in north-facing hillslopes (see Table 3). When interspersed sky cloudiness is considered during the snow season, for gaps sizes $D/H \geq 1$, NRSG again reduces monotonically with northward aspects, though at a smaller rate than in snow seasons with completely clear sky conditions. In small forest gaps ($D/H \leq 0.5$), the rates of change in S_{Net} and L_{Net} with varying aspects cancel each other out; and hence, NRSG expresses almost no variability with aspect as well as with gap size (Figure 8d). For all considered

©2014. American Geophysical Union. All Rights Reserved.

Table 3. Statistics of Minimum Net Radiation on Hillslopes of Different Aspects

Sky Condition	Orientation	$(D/H)_{min}$	Proportion of Radiation in Relation to Very Small Gaps (%)	Proportion of Radiation in Relation to Very Large Gaps (%)
Clear sky	South	0.5	91	34
	Southeast/West	0.5	90	36
	East/West	0.5	89	41
	Northeast/West	0.5	88	49
	North	0.5	87	53
Interspersed cloudy	South	0.1	100	47
	Southeast/West	0.1	100	48
	East/West	0.1	100	51
	Northeast/West	0.1	100	54
	North	0.1	100	57

aspects in interspersed cloudy snow seasons, the minimum radiation ($NRSG_{min}$) occurs at $(D/H)_{min} \approx 0.1$ on all hillslope orientations (Table 3).

3.4. Is a Forest Gap Always "Darker" Than Open Areas?

Sections 3.1, 3.2, and 3.3 highlight that at the study site, seasonal average net radiation reaching the forest gap is generally much less (i.e., it is "darker") than average net radiation in open areas (or a very large gap) for a wide range of gap sizes, hillslope angles, and orientations. However, considering that the relative dominance of S_{Net} and L_{Net} changes throughout the snow season, it is worth exploring if the magnitude of NRSG in a gap will ever be more than that in open areas and what are the controls on it. Additionally, within a gap, there are areas that have net radiation that is larger than open areas. To this end, here we first define two parameters to track the spatiotemporal variation of NRSG in forest gaps with respect to open areas: the daily averaged net radiation difference between the forest gap and open areas ($\Delta R = R_{gap} - R_{open}$ in $W\,m^{-2}$) and the percentage fraction of area receiving more radiation than open areas (Λ). The model is run for a range of gap sizes (including $D/H = 0.5$, 1, 2, 4, 10, and 20) on a level forest gap floor. For each case, temporal variations of ΔR and Λ are plotted daily during the snow season (Figures 9a and 10a). Since the difference in shortwave radiation between the gap and in open areas (ΔS_{Net}) is conversely proportional to the incoming shortwave radiation and the shading fraction, i.e., $\Delta S_{Net} \propto -\mathrm{SF}\,(S_{dir})_{open}$ (see equations (2) and (16)), as gap size increases, shading fraction decreases and hence ΔS_{Net} increases. For all gap sizes, ΔS_{Net} decreases with time (Figure 9a), with the largest decrease observed in small gaps. The decrease with time is because of the dominant effect of increasing $(S_{dir})_{open}$ (i.e., due to the decrease in Sun incidence angle) compared to changes in shading fraction with time late in the snow season. Between different gap sizes, the change in shading fraction with time is relatively larger in small gaps resulting in a larger decrease in ΔS_{Net}. It is noted than the nonsmooth variations of ΔS_{Net} and ΔR for all gap sizes are because of the uneven temporal variations in snow albedo (see Figure S1 in the supporting information). The difference in longwave component between the gap and open areas (ΔL_{Net}) can be expressed as: $(1 - \mathrm{SVF})(\sigma\varepsilon_{can}{T_{can}}^4 - \sigma\varepsilon_{sky}{T_{air}}^4)$ (see equations (2)–(10)). Since $\varepsilon_{can}{T_{can}}^4 > \varepsilon_{sky}{T_{air}}^4$ and also the difference between the two longwave components becomes larger with time due to the increase in air temperature and S_{Net}, ΔL_{Net} monotonically increases with time for all gap sizes (Figure 9a). Along similar lines, ΔL_{Net} decreases with an increase in gap size as SVF increases. Early in the snow season, ΔL_{Net} and its rate of change with D/H are larger than ΔS_{Net} and its change, and hence, ΔR decreases with increasing gap size. On the other hand, at the end of the snow season, the change in ΔS_{Net} with gap size is much larger than that in ΔL_{Net}, leading to a monotonically increasing ΔR with increasing gap size. As a result, ΔR in gaps of size $D/H \leq 10$ shows a monotonically decreasing variation with time; while in very large gaps ($D/H > 10$), ΔR expresses a minor variation with time (Figure 9a). Again, $\Delta R > 0$ indicates that daily spatially averaged net radiation in the gap is larger than in open areas. Results suggest that for $D/H \leq 10$, ΔR decreases with time and gradually becomes negative over the season, suggesting that the daily average net radiation in the forest gap is larger than that in open areas in the beginning of the season, but is less than that in open areas later in the season. Notably, the day (ξ) from the start of the season by which cumulative ΔR becomes equal to or larger than zero, is smaller for larger gaps for gap sizes $D/H \leq 10$ (Figures 9a and 11). This indicates that cumulative net radiation in very small gaps is larger than that in open areas for a longer period of time than in large gaps (e.g., $\xi = 51$ for

©2014. American Geophysical Union. All Rights Reserved.

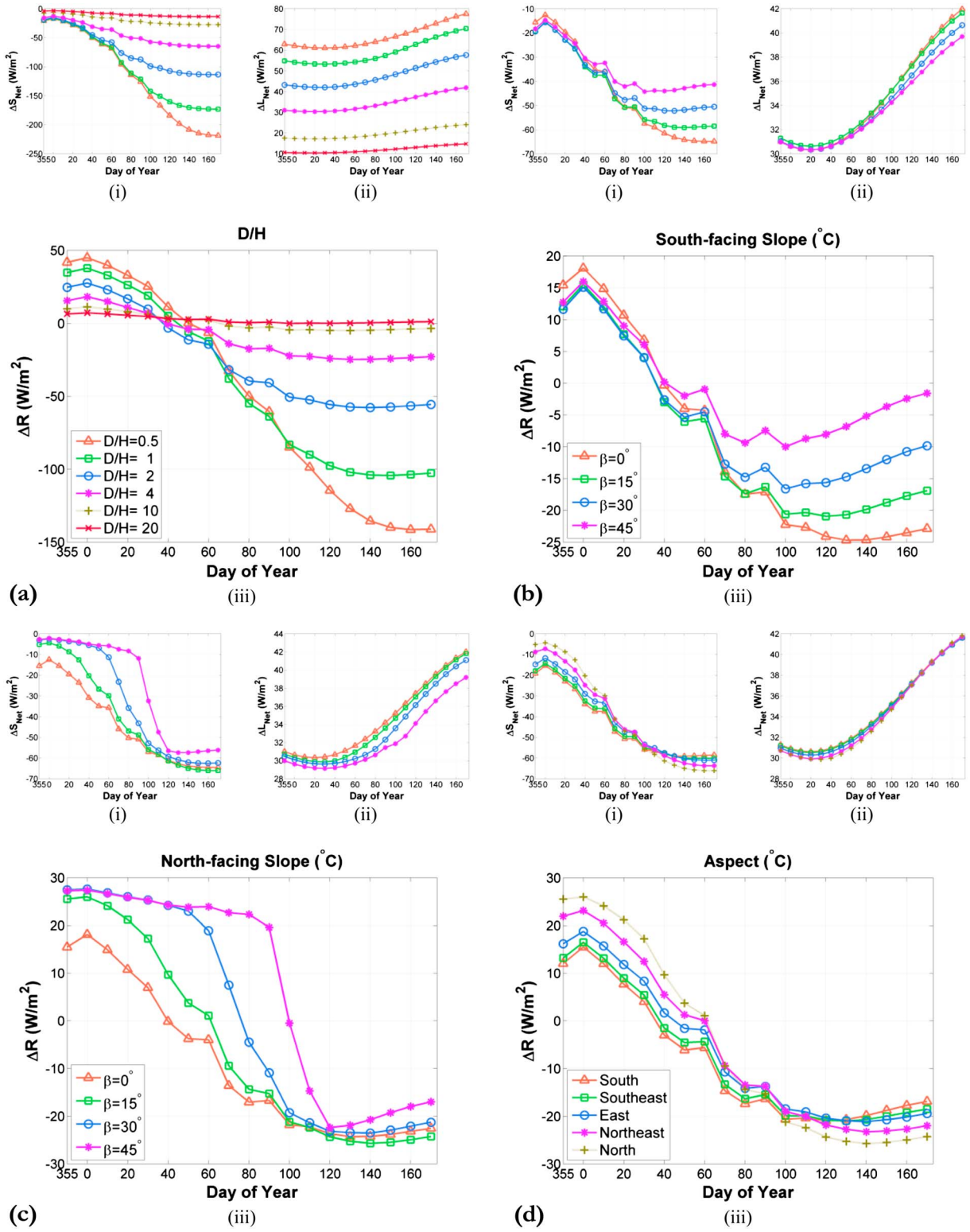

Figure 9. Variability of the difference between daily averaged radiation in the gap and the open area, $\Delta R = R_{gap} - R_{open}$, during the snow season for different (a) gap sizes, (b) south-facing slopes, (c) north-facing slopes, and (d) aspects. Figures 9b–9d were generated for $D/H = 4$.

©2014. American Geophysical Union. All Rights Reserved.

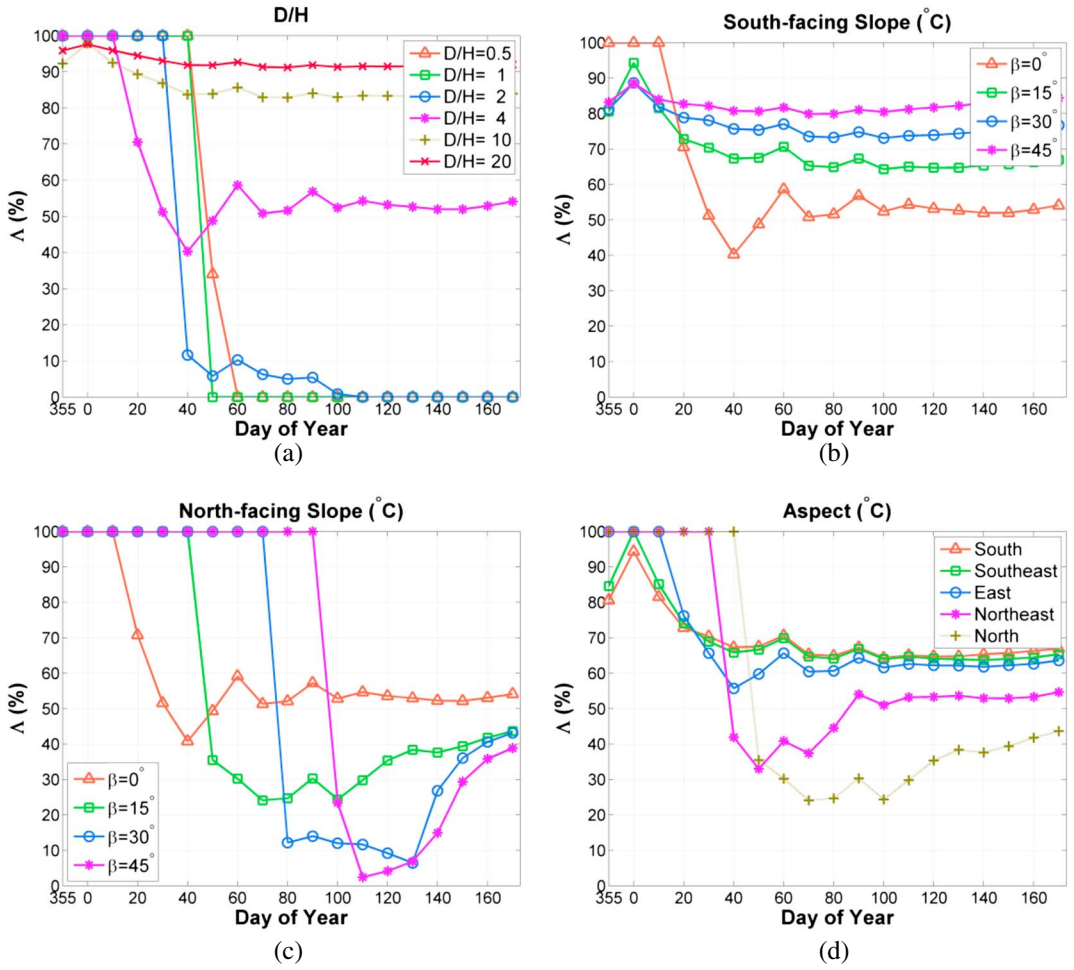

Figure 10. Variability of the portion of gap area which receives more radiation than open area, Λ, during the snow season for different (a) gap sizes, (b) south-facing slopes, (c) north-facing slopes, and (d) aspects.

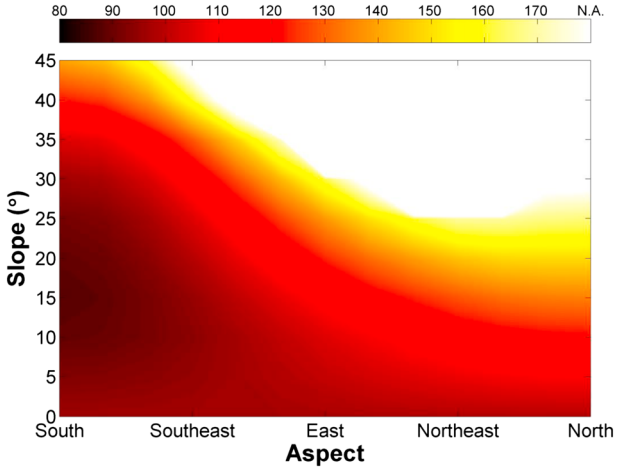

Figure 11. Effect of the duration of the snow season on NRSG's regime for different topographic characteristics for gap size $D/H = 4$. Contour colors show the day (ξ) until which the seasonal net radiation on the gap floor is larger than that in open areas. White areas indicate topographical conditions where NRSG is always larger than $NRSG_{open}$ over the season.

$D/H = 0.5$ relative to $\xi = 39$ for $D/H = 4$). In contrast, for gap sizes larger than $D/H = 10$, ξ is equal to zero thus indicating that larger gaps receive slightly more energy than that in open areas throughout the snow season. It is to be noted that even though the daily spatially averaged radiation within a gap may be larger or smaller than that in open areas, this relation may not hold true for the entire gap. The fraction of gap area that receives more radiation than in open areas, Λ, varies throughout the season with gap size (Figure 10a). For gap sizes with $D/H \leq 2$, the rapid decrease of ΔR with time (from positive to negative values) occurs in conjunction with the sharp decrease in Λ from 100% in the beginning to 0% later in the snow season. The fraction Λ in these small gaps is close to 100% in the beginning of the season, as net radiation in

©2014. American Geophysical Union. All Rights Reserved.

the gap is larger than that in open areas because of relatively dominant longwave radiation contribution from the canopy. In large gaps ($D/H \geq 10$), while ΔR for almost the entire gap is positive at all times during the season, there is a fraction of area (10% to 20%) near the southern edge of the gap where local ΔR is negative. This is mainly due to tree shading. Notably, late in the snow season when shortwave radiation is the dominant radiation contribution, as gap size increases, shading fraction decreases, and hence, Λ increases. The variation of Λ with time in intermediate forest gaps ($D/H = 4$) shows a decreasing followed by an increasing trend, before it plateaus late in the snow season. This is because earlier in the season, the variation of Λ is controlled by the longwave component, which decreases steadily until about day 30 at the study site because of reduction in air temperature with time. Later in the season, the shortwave radiation becomes the dominant component (because of increasing Sun angle and reduction in snow albedo) and hence Λ increases with time as shading fraction decreases until ΔR stabilizes, leading to minor variations in Λ.

In order to understand the influence of slope angle on the spatiotemporal variation of NRSG and consequently on when the seasonal net radiation in gap may be larger than that in open areas, ΔR and Λ are calculated for an intermediate-sized forest gap ($D/H = 4$) with varying slope angles (0°, 15°, 30°, and 45°) on both south-facing (Figures 9b and 10b) and north-facing (Figures 9c and 10c) hillslopes. As noted in section 3.2, solar incidence angle and shading fraction decrease with increasing south-facing slope angle, resulting in shortwave radiation on the forest gap floor and in open areas to increase with slope angle. Since the rate of change in shortwave radiation in the gap is different than that in open areas, ΔS_{Net} shows an irregular trend with slope angle in the beginning of the season. Early in the season when shading fraction is persistently large, incoming shortwave radiation increases with time, and hence, ΔS_{Net} decreases with time for all south-facing slope angles. Later in the season and particularly for large slopes, the rate of decrease in shading fraction with time becomes large enough, leading to a small increase in ΔS_{Net} with time. In contrast, for all south-facing slopes, ΔL_{Net} increases with time due to the increasing trend in air and canopy temperatures (similar to the explanation for Figure 9a). ΔL_{Net} does show minor variations with slope angles over the season due to changes in SVF and S_{Net} which in turn affects the canopy temperature. Because the variation in ΔS_{Net} with time is much larger than ΔL_{Net}, ΔR follows the variation of ΔS_{Net} with increasing slope angle and time. At the beginning of the season, ΔR decreases with time. Later in the season, ΔR increases with time and slope angle, as both ΔS_{Net} and ΔL_{Net} increase. Similar to ΔS_{Net}, ΔR increases with increasing slope angle (Figure 9b). As noted earlier, the nonsmooth variations of ΔS_{Net} and ΔR for all gap sizes are caused by the uneven temporal variations in snow albedo. The portion of gap that receives more radiation than open areas also varies with slope angle. As slope angle on south-facing hillslope increases, solar incidence angle decreases, and hence, shading fraction on the forest gap floor decreases, which results in an increasing Λ with slope angle. This is generally true over the snow season, except in early winter when longwave component is dominant (Figure 10b). On north-facing slopes, variation of ΔR and Λ are markedly different than that on south-facing slopes. Here incoming shortwave radiation both on the forest gap floor and in open areas decrease with increasing slope angle (increasing θ). At the beginning of the snow season, the rate of decrease in shortwave radiation on the forest gap floor is slower than that in open areas. As a result, ΔS_{Net} increases with slope angle. On higher slopes (30° and 45°), shortwave radiation mainly consists of diffuse radiation, and hence, ΔS_{Net} is close to zero. Since incoming shortwave radiation increases with time, ΔS_{Net} decreases until late in March and April, for all north-facing slopes. Late in the season, the rate of change in shortwave radiation for the gap and open areas become similar, $\Delta S_{\mathrm{Net}} \approx -57$ to $-64\ \mathrm{W\,m^{-2}}$, for different slope angles. Similar to south-facing slopes, ΔL_{Net} on north-facing slopes is conversely proportional to sky view factor and hence varies marginally with slope angle. As a result, ΔR follows the variation of ΔS_{Net} with time until late in March and April, when changes in ΔS_{Net} with slope is small. After March until the summer solstice, ΔR is controlled by ΔL_{Net}, and therefore, it gradually increases with time (Figure 9c).

Comparison of variation of ΔR between north-facing and south-facing hillslopes suggest that NRSG remains larger than that in open areas for a longer time on north-facing slopes than on south-facing slopes. For example, NRSG for a south-facing forest gap on 15° slope is larger than that for open areas until the 83rd day of the season. In contrast, for a 15° north-facing forest gap, NRSG remains larger than for open areas until day 133 of the snow season for an intermediate-sized forest gap ($D/H = 4$) (see Figure 11). ξ increases with increasing slope angle, for both south-facing and north-facing slopes. The portion of area receiving more radiation than open areas is also affected by changes in north-facing slope angle. In early winter, shortwave radiation is relatively small on north-facing slopes, both for gaps and open areas. Longwave radiation

©2014. American Geophysical Union. All Rights Reserved.

from canopy dominates net radiation on the forest gap floor, resulting in a larger NRSG than R_{open} over the entire forest gap floor (Λ = 100%). Later in the season, as solar elevation angle increases with time, Λ is controlled by shortwave radiation and shading fraction. As a result, Λ increases with time and decreases with slope angle (Figure 10c). Nonsmooth variations of snow albedo result in some irregularities in the overall trends during the spring period.

To understand the impact of hillslope aspect on spatiotemporal variability of net radiation and consequently on the period for which net radiation in gaps may be larger than that in open areas, ΔR and Λ are calculated for an intermediate-sized forest gap (D/H = 4) on five different hillslope (slope = 15°) aspects ranging from south, southeast/southwest, east/west, northeast/ northwest, and north-facing slopes. Due to the increase in incoming shortwave radiation with time, ΔS_{Net} decreases with time for all slope angles, during the winter. Changing the aspect affects ΔS_{Net} by influencing incoming shortwave radiation and shading fraction on the forest gap floor. As hillslope orientation changes from the south to the north, solar incidence angle and, hence, ΔS_{Net} increase. As solar elevation angle increases with time, the increase in shading fraction with increasing aspect becomes relatively dominant to the decrease in incoming shortwave radiation, resulting in a modest decrease in ΔS_{Net} with time. Due to the decrease in solar insolation with changing aspect from south to north, canopy temperature, and hence, ΔL_{Net} slightly decreases too. However, since $\Delta S_{Net} > \Delta L_{Net}$, ΔR increases with aspect in the beginning of the season (before day 75) and it decreases with aspect later in the season (after the 95th day). For the same reason, ΔR decreases with time until about the 75th day and then after day 140, it monotonically increases with time by the end of the season. In the winter period, the decrease of ΔS_{Net} with time is larger than the rate of increase in ΔL_{Net}, resulting in a decreasing ΔR. In the spring and early summer, variation of ΔL_{Net} is comparatively larger than that of ΔS_{Net}, leading to an increasing ΔR with time (Figure 9d). The cumulative ΔR is also strongly affected by changes in aspect. On south-facing slopes, it persistently remains negative almost over the entire season, which means the forest gaps are darker relative to open areas. However, on north-facing slopes, forest gaps are "brighter" than open areas (Figure 11). As discussed above, Λ on a south-facing hillslope decreases with time over the season. Changing the hillslope aspect also affects the portion of area, which receives more radiation than in open areas by varying shading fraction, incoming shortwave radiation and longwave radiation from canopy. During the summer, Λ is controlled by shortwave radiation gradients and shading fraction, leading to a decrease in Λ with northward orientation of hillslope. On the other hand, in the winter (when snow albedo is generally high) and particularly on north-facing slopes, the spatial distribution of radiation on the forest gap floor is dominated by longwave radiation from canopy, resulting in Λ = 100 for northeast/northwest and north-facing hillslopes (Figure 10d).

4. Conclusions

The study explored spatiotemporal gradients of net radiation reaching discontinuous forest gaps using a physically based model, GaRM, for a range of gap sizes and topographic configurations at a midlatitude site. Results showed that in small gaps ($D/H \leq 0.5$), net radiation on the forest gap floor is controlled by the longwave component with relatively small spatial gradients. However, in larger gaps ($D/H > 2$), the shortwave radiation dominantly governs the spatial pattern of net radiation and its trend with changing gap size. The spatial gradient of radiation (for gap size $D/H = 4$) is relatively muted for snow seasons with interspersed cloudy sky conditions, in relation to seasons with completely clear sky conditions.

Scenario experiments showed that the seasonal spatially averaged net radiation is minimized for relatively small gaps ($D/H = 0.5$) in level forests. The minimum radiation is observed to be about 11% less than net radiation in very small gaps and about 60% less than net radiation reaching the floor in open areas and very large gaps. The minimum seasonal net radiation persistently occurs for small gaps ($D/H \leq 0.5$) on both south-facing and north-facing forest slopes. Results also showed that forest gaps of size $D/H \leq 4$ are "dark" in the sense that seasonal net radiation in the gap is smaller than that in open areas. In contrast, gaps of size $D/H > 10$ receive a larger seasonal net radiation than in open areas. Although seasonally averaged net radiation is smaller than that in open areas for a wide range of gap sizes, the forest gap is not dark over the entire season and gap area. The research showed that the duration for which a "cold" gap may receive more radiation than open areas, varies with the slope and aspect of the hillslope. North-facing gaps tend to remain colder than open areas (i.e., receive less net radiation) for a shorter duration during the snow season, than south-facing slopes. This colder period shortens even further, with an increase in slope angle on

©2014. American Geophysical Union. All Rights Reserved.

north-facing slopes. In contrast, gaps on south-facing slopes receive less radiation than open areas for a longer time during the snow season. Along similar lines, fractional area of a forest gap that receives larger net radiation than in open areas also varies with time, gap size, slope, and aspect. The presented model and associated results will support better understanding and quantification of radiation-controlled processes such as snowmelt in snow-dominated patchy forests. The results could be applied to support optimal forest management practices to obtain the desired net radiation and hence melt regime on the forest gap floor by altering gap configurations. The topographic and meteorological dependence of net snowcover radiation further highlights the need to consider a wide range of factors in the prediction of water and energy fluxes in heterogeneous forests and for identification of best forest management strategies.

Acknowledgments

This study was supported by the Duke University start-up grant. Data sets used in the paper are mainly available to public from National Climatic Data Center (www.ncdc.noaa.gov) and National Renewable Energy Laboratory (www.nrel.gov). The data used for validating the model have been extracted from *Lawler and Link* [2011]. We also would like to thank Anne Nolin, Danny Marks, and one other anonymous reviewer for their constructive comments that greatly improved this manuscript.

References

Andreas, E. L. (1986), A new method of measuring the snow-surface temperature, *Cold Reg. Sci. Technol.*, *12*(2), 139–156.

Bernier, P. Y., and R. H. Swanson (1993), The influence of opening size on snow evaporation in the forests of the Alberta foothills, *Can. J. For. Res.*, *23*(2), 239–244.

Berry, G. J., and R. L. Rothwell (1992), Snow ablation in small forest openings in southwest Alberta, *Can. J. For. Res.*, *22*(9), 1326–1331.

Bohren, C. F., and D. B. Thorud (1973), 2 theoretical models of radiation heat-transfer between forest trees and snowpacks, *Agric. For. Meteorol.*, *11*(1), 3–16.

Brown, T. C., M. T. Hobbins, and J. A. Ramirez (2008), Spatial distribution of water supply in the coterminous United States, *J. Am. Water Resour. Assoc.*, *44*(6), 1474–1487.

de Chantal, M., K. Leinonen, T. Kuuluvainen, and A. Cescatti (2003), Early response of *Pinus sylvestris* and *Picea abies* seedlings to an experimental canopy gap in a boreal spruce forest, *For. Ecol. Manage.*, *176*(1–3), 321–336.

DeWalle, D. R., and A. Rango (2008), *Principles of Snow Hydrology*, vol. viii, pp. 410, Cambridge Univ. Press, Cambridge, U. K., and New York.

Douville, H., J. F. Royer, and J. F. Mahfouf (1995), A new snow parameterization for the Meteo-France climate model: 1. Validation in stand-alone experiments, *Clim. Dyn.*, *12*(1), 21–35.

Dozier, J., and S. G. Warren (1982), Effect of viewing angle on the infrared brightness temperature of snow, *Water Resour. Res.*, *18*(5), 1424–1434, doi:10.1029/WR018i005p01424.

Eck, T. F., and D. W. Deering (1990), Canopy albedo and transmittance in a boreal forest, *Remote Sens. Sci. Nineties*, *1–3*, 883–886.

Eck, T. F., and D. W. Deering (1992), Canopy albedo and transmittance in a spruce-hemlock forest in mid-September, *Agric. For. Meteorol.*, *59*(3–4), 237–248.

Ellis, C. R., and J. W. Pomeroy (2007), Estimating sub-canopy shortwave irradiance to melting snow on forested slopes, *Hydrol. Processes*, *21*(19), 2581–2593.

Ellis, C. R., J. W. Pomeroy, and T. E. Link (2013), Modeling increases in snowmelt yield and desynchronization resulting from forest gap-thinning treatments in a northern mountain headwater basin, *Water Resour. Res.*, *49*, 936–949, doi:10.1002/wrcr.20089.

Essery, R., J. Pomeroy, C. Ellis, and T. Link (2008a), Modelling longwave radiation to snow beneath forest canopies using hemispherical photography or linear regression, *Hydrol. Processes*, *22*(15), 2788–2800.

Essery, R., P. Bunting, J. Hardy, T. Link, D. Marks, R. Melloh, J. Pomeroy, A. Rowlands, and N. Rutter (2008b), Radiative transfer modeling of a coniferous canopy characterized by airborne remote sensing, *J. Hydrometeorol.*, *9*(2), 228–241.

Flerchinger, G. N., W. Xaio, D. Marks, T. J. Sauer, and Q. Yu (2009), Comparison of algorithms for incoming atmospheric long-wave radiation, *Water Resour Res.*, *45*, W03423, doi:10.1029/2008WR007394.

Gardner, A. S., and M. J. Sharp (2010), A review of snow and ice albedo and the development of a new physically based broadband albedo parameterization, *J. Geophys. Res.*, *115*, F01009, doi:10.1029/2009JF001444.

Gary, H. L. (1974), Snow accumulation and snowmelt as influenced by a small clearing in a lodgepole pine forest, *Water Resour. Res.*, *10*(2), 348–353, doi:10.1029/WR010i002p00348.

Golding, D. L., and R. H. Swanson (1978), Snow accumulation and melt in small forest openings in Alberta, *Can. J. For. Res.*, *8*(4), 380–388.

Gryning, S. E., E. Batchvarova, and H. A. R. De Bruin (2001), Energy balance of a sparse coniferous high-latitude forest under winter conditions, *Boundary Layer Meteorol.*, *99*(3), 465–488.

Hardy, J. P., R. E. Davis, R. Jordan, X. Li, C. Woodcock, W. Ni, and J. C. McKenzie (1997), Snow ablation modeling at the stand scale in a boreal jack pine forest, *J. Geophys. Res.*, *102*(D24), 29,397–29,405, doi:10.1029/96JD03096.

Hardy, J. P., R. Melloh, G. Koenig, D. Marks, A. Winstral, J. W. Pomeroy, and T. Link (2004), Solar radiation transmission through conifer canopies, *Agric. For. Meteorol.*, *126*(3–4), 257–270.

Hedstrom, N. R., and J. W. Pomeroy (1998), Measurements and modelling of snow interception in the boreal forest, *Hydrol. Processes*, *12*(10–11), 1611–1625.

Hottel, H. C. (1976), Simple model for estimating transmittance of direct solar-radiation through clear atmospheres, *Sol. Energy*, *18*(2), 129–134.

Huemmrich, K. F. (2001), The GeoSail model: A simple addition to the SAIL model to describe discontinuous canopy reflectance, *Remote Sens. Environ.*, *75*(3), 423–431.

Kalogirou, S. (2009), *Solar Energy Engineering: Processes and Systems*, vol. xv, pp. 760, Elsevier/Academic Press, Burlington, Mass.

Kimball, B. A., S. B. Idso, and J. K. Aase (1982), A model of thermal-radiation from partly cloudy and overcast skies, *Water Resour. Res.*, *18*(4), 931–936, doi:10.1029/WR018i004p00931.

Kreith, F., and J. F. Kreider (2011), *Principles of Sustainable Energy*, vol. xxiii, 855 p., 816 p. of plates pp., CRC Press, Boca Raton, Fla.

Kumar, L., A. K. Skidmore, and E. Knowles (1997), Modelling topographic variation in solar radiation in a GIS environment, *Int. J. Geogr. Inf. Sci.*, *11*(5), 475–497.

Lawler, R. R., and T. E. Link (2011), Quantification of incoming all-wave radiation in discontinuous forest canopies with application to snowmelt prediction, *Hydrol. Processes*, *25*(21), 3322–3331.

Liang, S. L., and A. H. Strahler (1994), A stochastic radiative-transfer model of a discontinuous vegetation canopy, IGARSS '94 - 1994, *Int. Geosci. Remote Sens. Symp.*, *1–4*, 1626–1628.

Link, T., and D. Marks (1999), Distributed simulation of snowcover mass- and energy-balance in the boreal forest, *Hydrol. Processes*, *13*(14–15), 2439–2452.

Male, D. H., and R. J. Granger (1981), Snow surface-energy exchange, *Water Resour. Res.*, *17*(3), 609–627, doi:10.1029/WR017i003p00609.

©2014. American Geophysical Union. All Rights Reserved.

Marks, D., and J. Dozier (1979), Clear-sky longwave radiation model for remote alpine areas, *Arch. Meteorol. Geophys. B*, *27*(2–3), 159–187.
Marthews, T. R., Y. Malhi, and H. Iwata (2012), Calculating downward longwave radiation under clear and cloudy conditions over a tropical lowland forest site: An evaluation of model schemes for hourly data, *Theor. Appl. Climatol.*, *107*(3–4), 461–477.
Matzarakis, A., and O. Matuschek (2011), Sky view factor as a parameter in applied climatology—Rapid estimation by the SkyHelios model, *Meteorol. Z.*, *20*(1), 39–45.
National Climatic Data Center (2014). [Available at http://www.ncdc.noaa.gov/oa/ncdc.html, Accessed July, 2012.]
Nilson, T. (1971), A theoretical analysis of the frequency of gaps in plant stands, *Agric. For. Meteorol.*, *8*(0), 25–38.
National Renewable Energy Laboratory (NREL) (2014). [Available at www.nrel.gov, Accessed February 2013.]
Pluss, C., and A. Ohmura (1997), Longwave radiation on snow-covered mountainous surfaces, *J. Appl. Meteorol.*, *36*(6), 818–824.
Pomeroy, J. W., A. Rowlands, J. Hardy, T. Link, D. Marks, R. Essery, J. E. Sicart, and C. Ellis (2008), Spatial variability of shortwave irradiance for snowmelt in forests, *J. Hydrometeorol.*, *9*(6), 1482–1490.
Pomeroy, J. W., D. Marks, T. Link, C. Ellis, J. Hardy, A. Rowlands, and R. Granger (2009), The impact of coniferous forest temperature on incoming longwave radiation to melting snow, *Hydrol. Processes*, *23*(17), 2513–2525.
Prata, A. J. (1996), A new long-wave formula for estimating downward clear-sky radiation at the surface, *Q. J. R. Meteorol. Soc.*, *122*(533), 1127–1151.
Seyednasrollah, B., and M. Kumar (2013), Effects of tree morphometry on net snow cover radiation on forest floor for varying vegetation densities, *J. Geophys. Res. Atmos.*, *118*, 12,508–12,521, doi:10.1002/2012JD019378.
Seyednasrollah, B., M. Kumar, and T. E. Link (2013), On the role of vegetation density on net snow cover radiation at the forest floor, *J. Geophys. Res. Atmos.*, *118*, 8359–8374, doi:10.1002/jgrd.50575.
Sicart, J. E., J. W. Pomeroy, R. L. H. Essery, and D. Bewley (2006), Incoming longwave radiation to melting snow: Observations, sensitivity and estimation in northern environments, *Hydrol. Processes*, *20*(17), 3697–3708.
Song, C. H., and L. E. Band (2004), MVP: A model to simulate the spatial patterns of photosynthetically active radiation under discrete forest canopies, *Can. J. For. Res.*, *34*(6), 1192–1203.
Sproles, E. A., A. W. Nolin, K. Rittger, and T. H. Painter (2013), Climate change impacts on maritime mountain snowpack in the Oregon Cascades, *Hydrol. Earth Syst. Sci.*, *17*(7), 2581–2597.
Strack, J. E., G. E. Liston, and R. A. Pielke (2004), Modeling snow depth for improved simulation of snow-vegetation-atmosphere interactions, *J. Hydrometeorol.*, *5*(5), 723–734.
Susong, D., D. Marks, and D. Garen (1999), Methods for developing time-series climate surfaces to drive topographically distributed energy- and water-balance models, *Hydrol. Processes*, *13*(12–13), 2003–2021.
Todhunter, P. E., F. Xu, and J. M. Buttle (1992), A model of Net-radiation over suburban snowpacks, *Atmos. Environ. B-Urb.*, *26*(1), 17–27.
Varhola, A., N. C. Coops, M. Weiler, and R. D. Moore (2010), Forest canopy effects on snow accumulation and ablation: An integrative review of empirical results, *J. Hydrol.*, *392*(3–4), 219–233.
Warren, S. G. (1982), Optical-properties of snow, *Rev. Geophys.*, *20*(1), 67–89, doi:10.1029/RG020i001p00067.
Wong, L. T., and W. K. Chow (2001), Solar radiation model, *Appl. Energy*, *69*(3), 191–224.

©2014. American Geophysical Union. All Rights Reserved.